

# Effect of $\delta$ phase precipitation on grain growth and mechanical properties of Inconel 718 prepared by selective laser melting

Mingbo Na<sup>1</sup>, Yiqiang Mu<sup>2,3</sup>, Mingchuan Zhang<sup>2</sup>, Jinbao Hu<sup>2</sup>, Shaowei Lu<sup>1</sup>, Qinsi Xu<sup>2,3\*</sup>

<sup>1</sup>College of Aerospace Engineering, Shenyang Aerospace University, Shenyang 110136, P. R. China

<sup>2</sup>College of Civil Aviation, Shenyang Aerospace University, Shenyang 110136, P. R. China

<sup>3</sup>Institute of Metal Research, Chinese Academy of Sciences, Shenyang 110016, P. R. China

Received 29 December 2022, received in revised form 22 April 2023, accepted 6 March 2024

## Abstract

Selective laser melting (SLM) is widely used for forming metals due to its complexity in geometrical design. Defects are unavoidably introduced in the manufacturing process, which requires post-processing. But it leads to grain growth. In this work, a series of post-heat treatments were used to study the effect of  $\delta$  phase precipitation on grain growth and mechanical properties in SLM Inconel 718. Optical microscopy (OM), scanning electron microscopy (SEM) and X-ray diffraction (XRD) were used to study the microstructure of the specimens. The results showed that the precipitation of the  $\delta$  phase increased with increasing aging time and that the growth of grains was inhibited by the  $\delta$  phase. After 750 °C pre-aging for 48 h, the solution-treated specimen had the optimum strength and plasticity.

Key words:  $\delta$  phase, grain growth, SLM, Inconel 718, heat treatment

## 1. Introduction

Ni-based superalloys are extensively used in gas turbine disks, rocket motors, spacecraft and nuclear reactors due to their outstanding oxidation resistance, corrosion resistance, and mechanical properties. The Ni-Cr-Fe-based Inconel 718 alloy is the most widely used superalloy because of its capacity to maintain microstructural stability up to 650 °C. Inconel 718 with the austenite matrix  $\gamma$  phase is strengthened by the principal strengthening  $\gamma''$  phase [1]. However, its high hardness and low thermal conductivity characteristics make it difficult to apply conventional machining methods owing to tool over-wear and poor workpiece surface integrity [2]. The actual components have a variety of complex shapes, and the use of traditional casting or forging has difficulty meeting the requirements. Metal additive manufacturing is an advanced manufacturing method which allows the building of diverse parts, from either powders or wire feedstock, with good accuracy and directly from a computer CAD model without any part-specific tooling or knowledge [3]. Selective laser melting technology is often used in the AM of metal materials, fabricat-

ing components according to a high-energy laser to melt metal powders layer by layer. Complex geometrical parts with high dimensional accuracy and good surface integrity can be accurately obtained without subsequent technological requirements, which is difficult to achieve by traditional methods [2]. Nevertheless, porosity, residual stress and segregation regions may occur in the SLM process [4]. Many experimental investigations have been conducted regarding the microstructures and mechanical properties of laser-processed Inconel 718 components. Popovich et al. [5] obtained the microstructure by applying HIP + H/T post-processing. The mechanical properties became superior to those of cast and wrought Inconel 718. Li et al. [6] found that the hardness of the alloy first increased and then decreased with increasing solution temperature under the same aging conditions. However, the post-process may cause grain coarsening and affect the mechanical properties [7, 8].

The  $\delta$  phase plays an important role in Inconel 718, and grain growth can be inhibited by controlling  $\delta$  phase precipitation. Wang et al. [9] employed a two-stage annealing treatment in Ni-based superalloy, and the result showed that mixed grains could be refined

\*Corresponding author: e-mail address: [20180062@sau.edu.cn](mailto:20180062@sau.edu.cn)

Table 1. The chemical composition of Inconel 718 alloy powder (wt.%)

Ni	Cr	Nb	C	Mn	Mo	Co	Al	Ti	Si	Cu	Fe
52.34	18.68	4.91	0.038	0.031	3.26	0.14	0.43	0.93	0.09	0.018	Bal.

Table 2. Heat treatment procedures used on SLM Inconel 718

Designation	Aging	Solution treatment
as-built	–	–
DA-2	750 °C × 8 h, AC	–
DA-3	750 °C × 24 h, AC	–
DA-4	750 °C × 48 h, AC	–
AS-1	–	1000 °C × 2 h, AC
AS-2	750 °C × 8 h, AC	1000 °C × 2 h, AC
AS-3	750 °C × 24 h, AC	1000 °C × 2 h, AC
AS-4	750 °C × 48 h, AC	1000 °C × 2 h, AC

and homogenized by precipitating some  $\delta$  phases at a suitable aging annealing treatment and a relatively high recrystallization annealing treatment. The pre-precipitated  $\delta$  phase promotes the nucleation of static recrystallization and slows down the growth of grains [10]. There are many works about the grain growth of cast or wrought Inconel 718 [11–15], but a few about SLM-IN718. In this paper, the microstructures and  $\delta$  phase precipitation under different heat treatments were investigated. Then, hardness and stress rupture testing were further conducted to study the effects of the  $\delta$  phase on grain growth and mechanical properties.

## 2. Materials and methods

Gas-atomized IN718 powders with particle sizes from 15 to 45  $\mu\text{m}$  were used in the experiment, and the morphology of the IN718 powders is shown in Fig. 1a. The chemical composition (wt.%) of the powders is shown in Table 1. The specimens were fabricated on an SLM metal 3D printer (EOS 280) with a fiber laser with a power of  $\sim 400$  W, and the manufacturer's recommended printing parameters were used. During fabrication by SLM, a standard alternating  $x/y$  raster strategy was chosen. This strategy features bidirectional hatches of a layer ' $n$ ' performed in the  $x$ -direction whilst the next layer ' $n+1$ ' turned  $90^\circ$  [16]. The final two kinds of dimensions of the specimens were  $10 \times 10 \times 10 \text{ mm}^3$  and  $15 \times 15 \times 15 \text{ mm}^3$ , and the microstructure specimen and tensile specimen are shown in Fig. 1b. The specimens were aged at  $750^\circ\text{C}$  and then solution treated at  $1000^\circ\text{C}$  to investigate the effect of  $\delta$  phase precipitation on grain growth. Different heat treatments are listed in Table 2.

The microstructure of the specimens was investigated with a COIC-900 Optical Microscope. X-ray

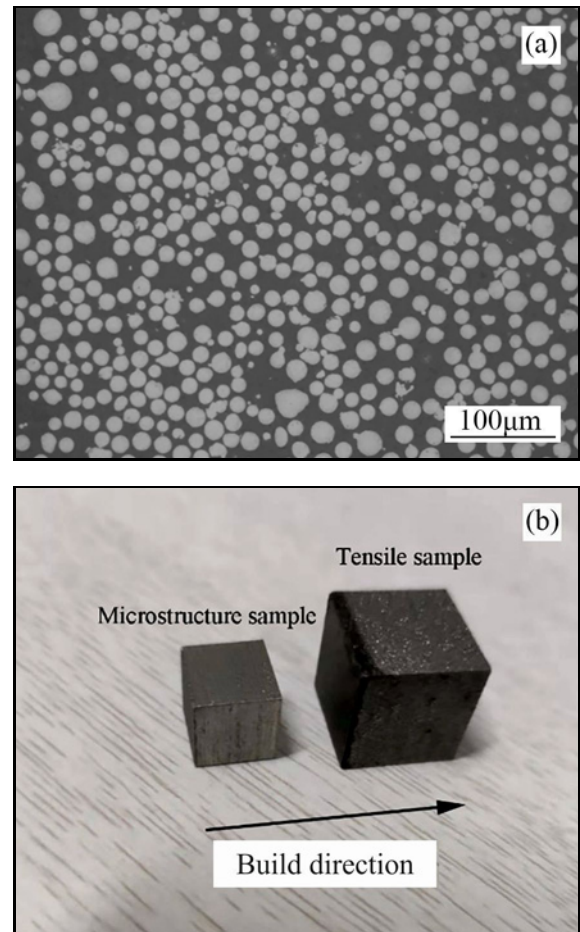


Fig. 1. (a) IN718 powders morphology and (b) the as-built microstructures and tensile specimens.

diffraction patterns were obtained using a Bruker D8 diffractometer with  $\text{CoK}\alpha$  radiation ( $\lambda = 1.790307 \text{ \AA}$ ). Diffraction patterns were recorded within the  $2\theta$  range

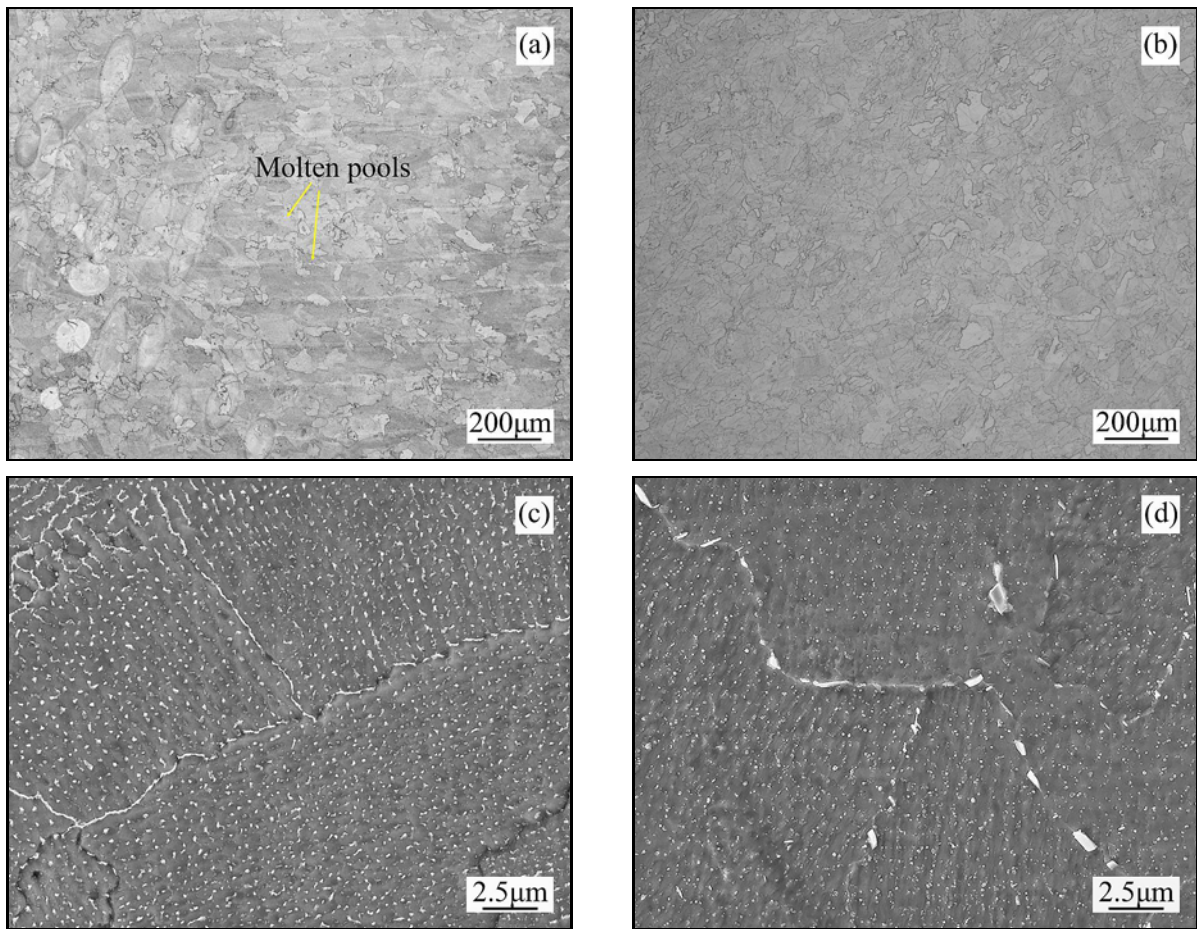


Fig. 2. The microstructures of the top surface of the (a), (c) as-built and (b), (d) AS-1 specimens.

from  $40^\circ$  to  $115^\circ$  with a step size of  $0.005^\circ$ . Tescan Mira3 Scanning Electron Microscope was equipped with an Ultim MaxN Energy Dispersive Spectroscopy detector. The specimens were successively prepared with waterproof abrasive papers from 800 to 2000 grit for metallographic observation. Mechanical polishing was performed using a diamond suspension with a  $0.05 \mu\text{m}$  colloidal silica suspension. Then, the specimens were etched with a Kallings etchant of a solution of 100 ml  $\text{C}_2\text{H}_5\text{OH}$  + 100 ml  $\text{HCl}$  + 5 g  $\text{CuCl}_2$ . The Vickers hardness tests were carried out using an HVS-1000A microhardness tester at a load of 200 g and an indentation time of 10 s. The tensile specimens were cut into dog-bone shapes from the build cubes (Fig. 2b), with gauge dimensions of 3 mm in length, 1 mm in width, and  $200 \mu\text{m}$  in thickness [17]. The dog-bone shape tensile specimens were electropolished in a solution of 10 ml  $\text{HClO}_4$  + 90 ml  $\text{C}_2\text{H}_5\text{OH}$ , which was tested under uniaxial tension along the building direction in an Instron 1000 tester at a strain rate of  $5 \times 10^{-4} \text{s}^{-1}$  at room temperature.

### 3. Results and discussion

#### 3.1. Microstructures of as-built and direct solution specimens

The alloy powders were melted directly with a high-energy laser beam in the SLM process. Figure 2 shows the microstructure of the as-built and AS-1 specimens. The molten pool boundary was formed when the laser passed through adjacent metal powders twice. The molten pool completely disappeared after solution treatment, which means that recrystallization occurred. The same phenomenon was also observed at  $1050^\circ\text{C}$  [4]. The chains of the Laves phase can be seen in intragranular and grain boundaries, which become granular after 2 h at  $1000^\circ\text{C}$  (Figs. 2c,d) [18]. As shown in Fig. 3, the  $\gamma$  phase has strong peaks, while the Laves phase shows weak peaks. But no peaks of the  $\delta$  phase were detected. The  $\delta$  phase cannot precipitate during the SLM process, which is responsible for the high cooling rate and Nb consumption of the Laves phase.

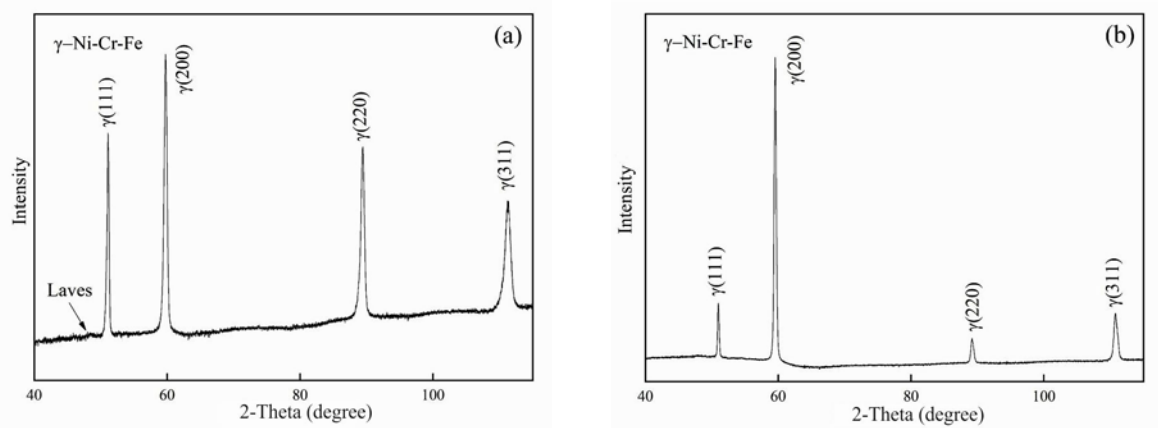


Fig. 3. XRD patterns of (a) as-built and (b) AS-1 specimens.

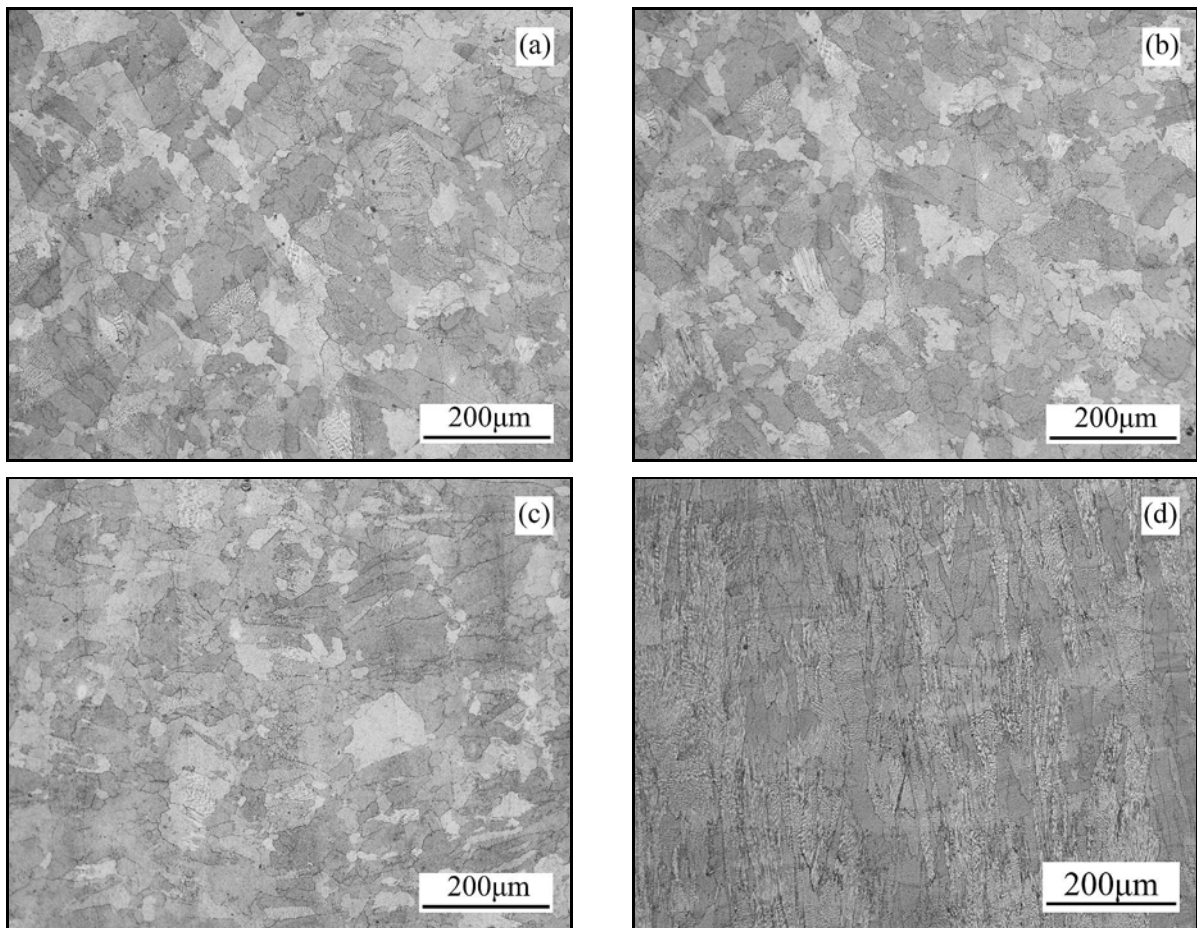


Fig. 4a–d. Top, side surfaces, and corresponding microstructures of (a) and (d) DA-2, (b) DA-3, (c) DA-4 specimens.

### 3.2. $\delta$ phase precipitation under different heat treatments

To obtain different amounts of the  $\delta$  phase, the specimens were aged at 750 °C for 8, 24, and 48 h. Figure 4 shows the metallographic structures of the specimens under different aging times. The microstructures

after heat treatment maintained a similar morphology to the as-built specimen, and molten pools still existed. In SLM-IN718, grains are columnar and parallel to the build direction. Equiaxed grains can be seen on the top surfaces (Figs. 4a–c), and the side surfaces are columnar (Figs. 4b–f). The rapid cooling rate and large temperature gradient lead to the orientation of

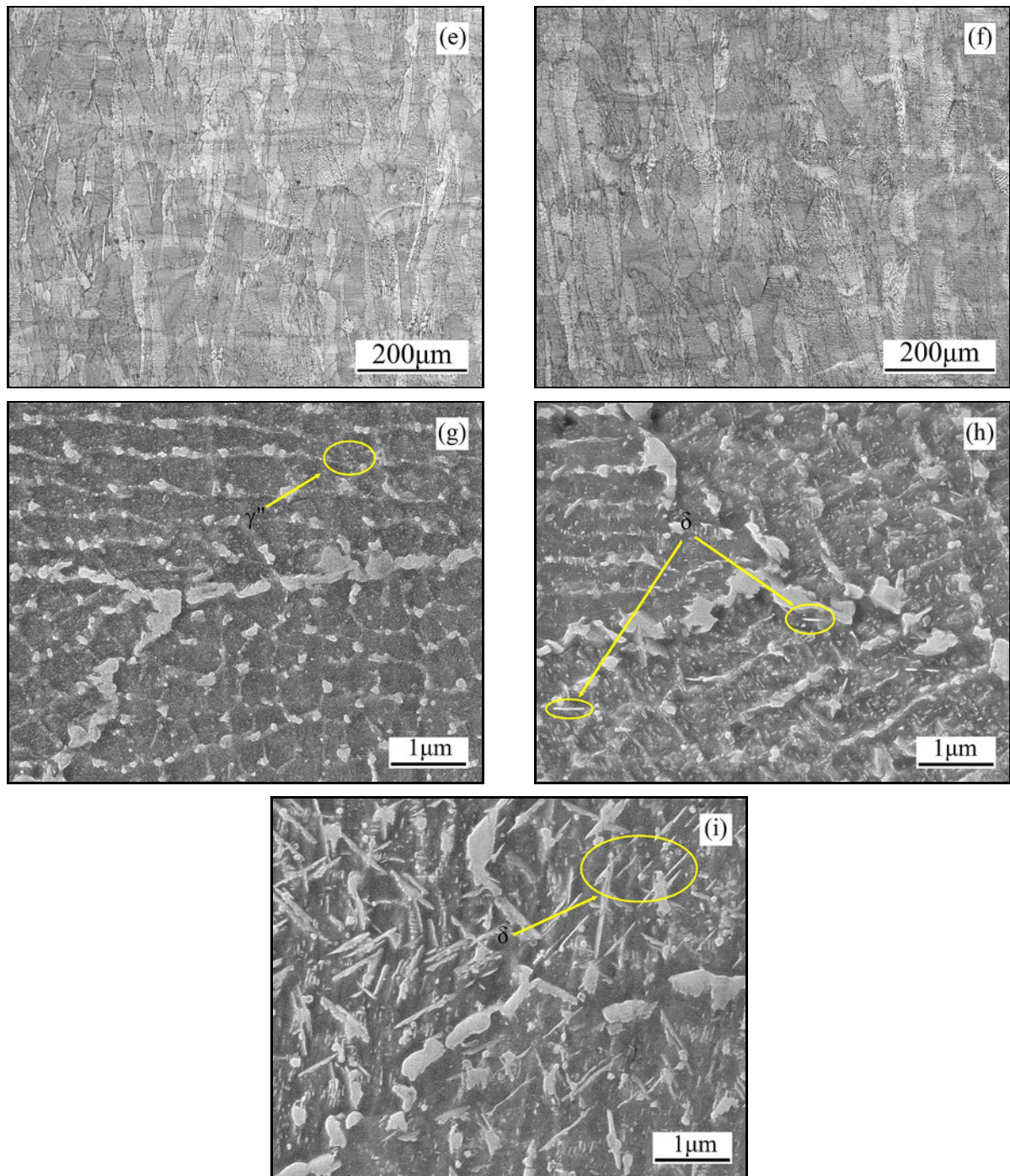


Fig. 4g-i. Top, side surfaces, and corresponding microstructures of (g) DA-2, (e) and (h) DA-3 specimens, (e) and (f) DA-4 specimens.

grain growth in the SLM process. Figures 4g-i show that the chain Laves phase decreased with increasing aging time. The  $\gamma''$  phase became coarse, and more  $\delta$  phase precipitated. The  $\delta$  phase precipitates faster at 750 °C than 700 °C [19]. Higher grain boundary energy causes a favorable nucleation site of the  $\delta$  phase. At low temperatures, the transition from  $\gamma''$  to  $\delta$  starts from the grain boundary through cell reaction, while the high-angle grain boundary increases [20, 21]. The

energy barrier of the  $\gamma''$  phase is lower than that of  $\delta$  phase, so the  $\delta$  phase precipitates later than the  $\gamma''$  phase. Then, the unstable  $\gamma''$  phase translates into the stable  $\delta$  phase. Zhang et al. [22] found that the  $\gamma''$  phase lost its coherent relationship with the matrix as the  $\gamma''$  phase coarsened, and the coarsening process of the  $\gamma''$  phase in IN718 was controlled by the volume diffusion of Nb atoms in the matrix. Figure 5 shows the EDS analysis of the  $\delta$  phase in the DA-4 specimen,

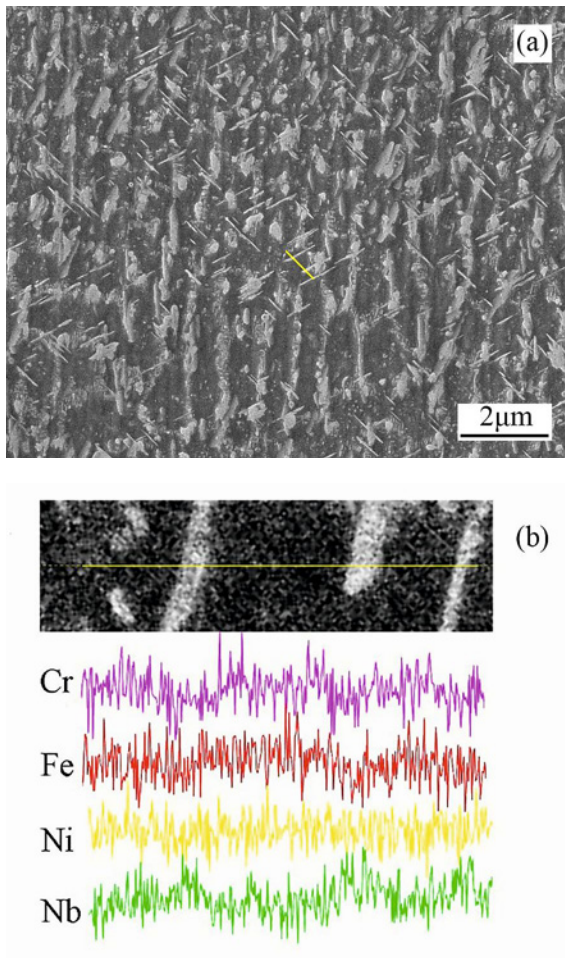


Fig. 5. (a) The  $\delta$  phase in DA-4 specimens and (b) EDS map.

which shows that Nb is the main element of the phase. The  $\delta$  phase precipitates next to the partially melted Laves phase. Zhang et al. [23] noted Nb diffusion in the dissolution process of the Laves phase. This promoted the formation of  $\gamma''$  and the transformation of  $\gamma'' \rightarrow \delta$ .

Typical XRD patterns of SLM-processed Inconel 718 are depicted in Fig. 6, which are in good agreement with some previous investigations on the constitutional phases of laser-processed Inconel 718 [24, 25]. In general, strong diffraction peaks corresponding to the  $\gamma$  matrix with an A1-ordered face-centered cubic (fcc) crystal structure, and  $\gamma''$   $\text{Ni}_3\text{Nb}$  in a body-centered tetragonal (bct) crystal structure were detected. There was no precipitated  $\delta$  phase after aging at 750 °C for 8 h, but a few  $\delta$  phases precipitated after aging at 750 °C for 24 h. Significant precipitated peaks were detected after aging at 750 °C for 48 h, which meant that a large amount of the  $\delta$  phase precipitated.

Molten pools cannot be observed in Figs. 7a–f af-

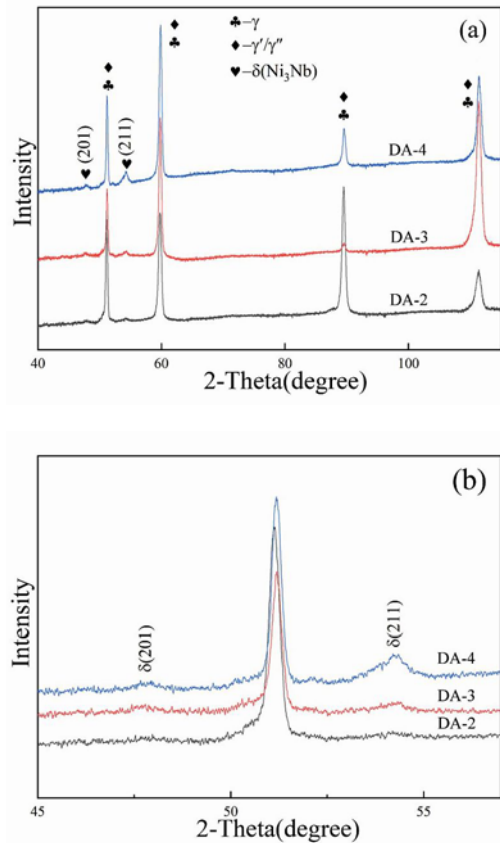


Fig. 6. XRD patterns of (a) DA-2, DA-3, and DA-4 specimens and (b) their partially enlarged detail.

ter 1000 °C solution treatment. The grain size and the number of abnormally grown grains decrease with increasing pre-aging time. As indicated by the arrow in Fig. 7a, the partially dissolved Laves phase can be observed. The  $\gamma''$  phase disappeared after solution treatment at 1000 °C, whose dissolving temperature is 870~930 °C [26]. The  $\delta$  phase dissolved after solution treatment at 1000 °C, and the pinning effect of the  $\delta$  phase on the grain boundary was weak. The grain can easily grow and coarsen. There are a few short-rod  $\delta$  phases in the AS-4 specimen (Fig. 7i), and weak peaks of the  $\delta$  phase can still be observed (see Fig. 8b). It might be that the superabundant  $\delta$  phase was not completely dissolved with aging at 750 °C for 48 h. Many studies [24, 27–29] have indicated that the grain coarsening phenomenon is not obvious when the solution temperature is between 980 and 1020 °C. In addition, higher temperatures can provide more energy for grain growth. The  $\delta$  phase was completely dissolved and could not pin the grain boundary or inhibit grain growth. The above results show that increasing aging time increases the precipitation of the phase, and the grains are refined.

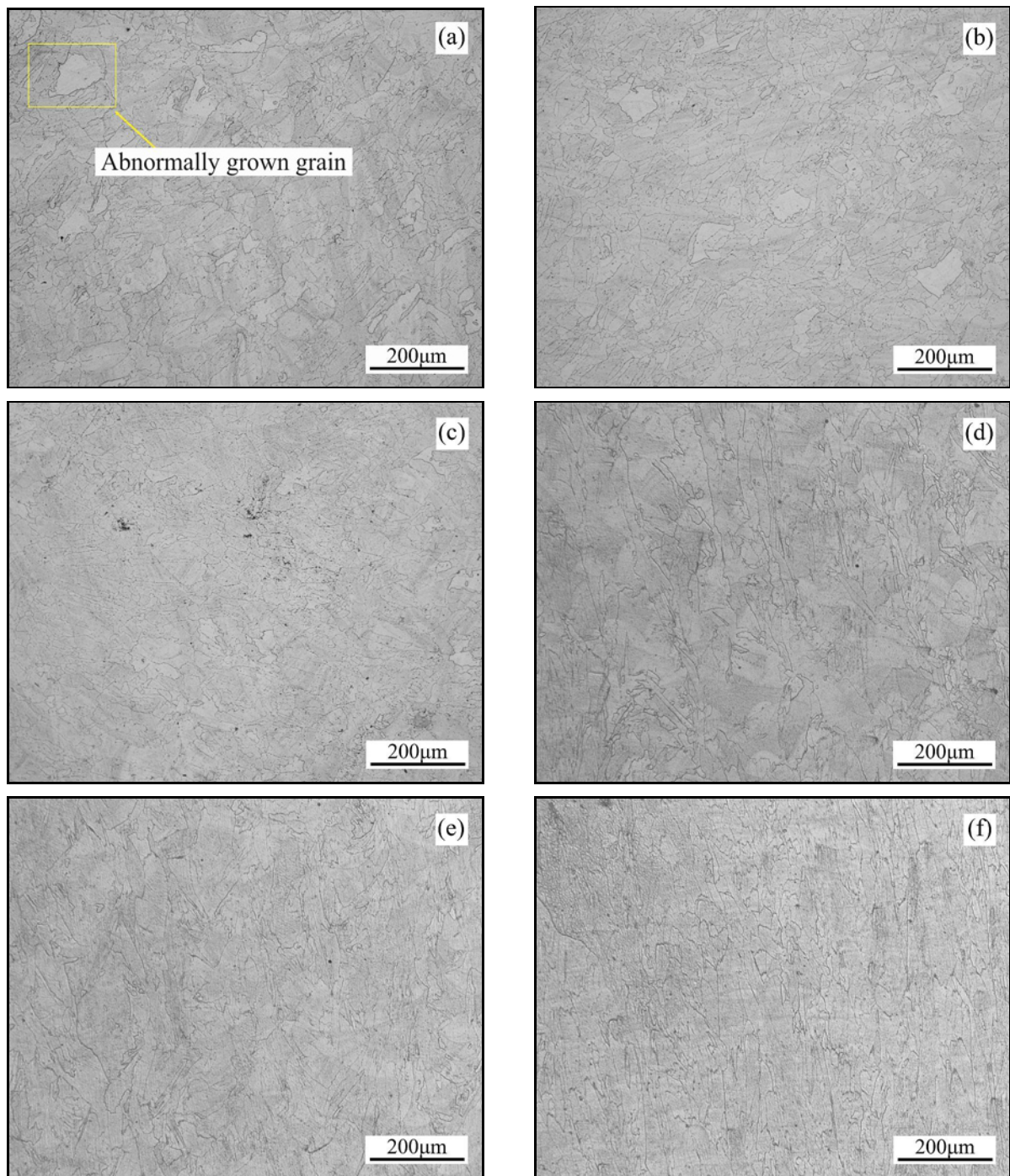


Fig. 7a–f. Top, side surfaces, and corresponding microstructures of (a) and (d) AS-2, (b) and (e) AS-3, (c), (e) and (f) AS-4 specimens.

### 3.3. Mechanical properties of different heat treatment specimens

Vickers hardness tests and tensile tests were carried out to study the mechanical properties. Figure 9a shows the microhardness on the top surfaces of SLM-IN718. The maximum value is DA-4 (416 HV), followed by as-built (316 HV). The microhardness of AS-1 and AS-4 is the lowest (270 and

285 HV). After the aging treatment, the microhardness of the DA-4 specimen experienced a significant increase (32 %) compared to the as-built specimen. Much of the  $\delta$  phase precipitated during aging treatment for 48 h and improved the microhardness of the specimen. Compared with the as-built specimen, the microhardness of AS-1 and AS-4 decreased by 15 and 10 %, respectively, because almost all that remained was the  $\gamma$  matrix after 1000 °C solution treatment (see

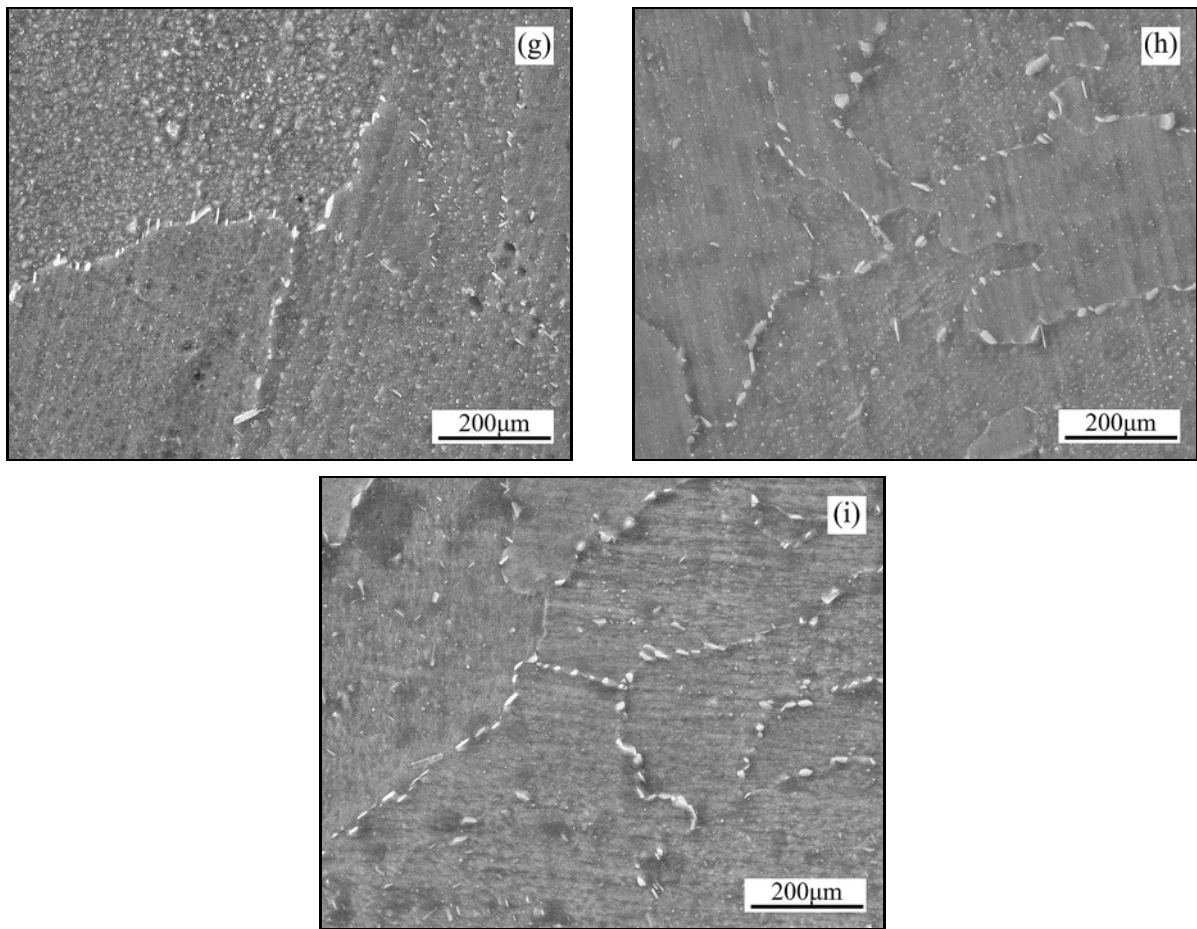


Fig. 7g–i. Top, side surfaces, and corresponding microstructures of (g) AS-2, (h) AS-3 specimens, and (i) the short-rod  $\delta$  phases in the AS-4.

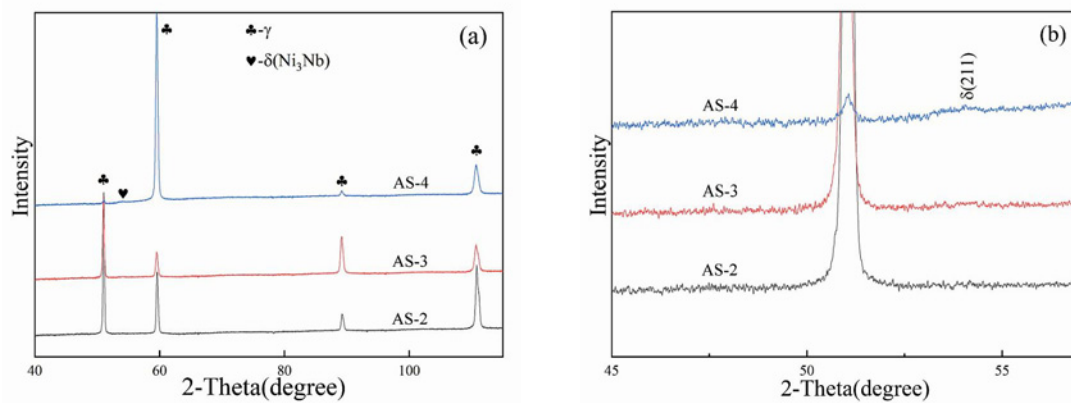


Fig. 8. XRD patterns of AS-2, AS-3, and AS-4 specimens.

Fig. 2d). The undissolved  $\delta$  phase (Fig. 8b) in AS-4 resulted in a higher microhardness than AS-1.

The tensile test results of SLM-IN718 are presented in Fig. 9b. Both the AS-1 and AS-4 specimens exhibit better ductility than the as-built and DA-4 specimens, while the ultimate strength and yield strength are obviously disadvantaged compared to DA-4. The precip-

itation of the  $\gamma''$  and  $\delta$  phases improved the strength of the alloy in the aging process, but all the strengthening phases dissolved after solution treatment. Both the ductility and strength of DA-4 are superior to those of DA-1. DA-4 experienced a pre-aging process for 48 h, which precipitated more  $\delta$  phase. The  $\delta$  phase can improve the nucleation rate during recrystallization and

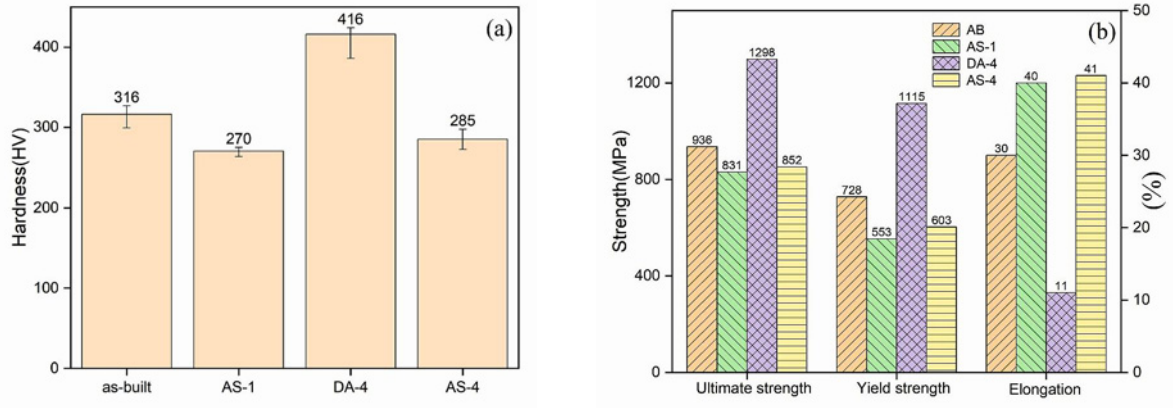


Fig. 9. Mechanical properties of SLM-Inconel 718 under different heat treatments.

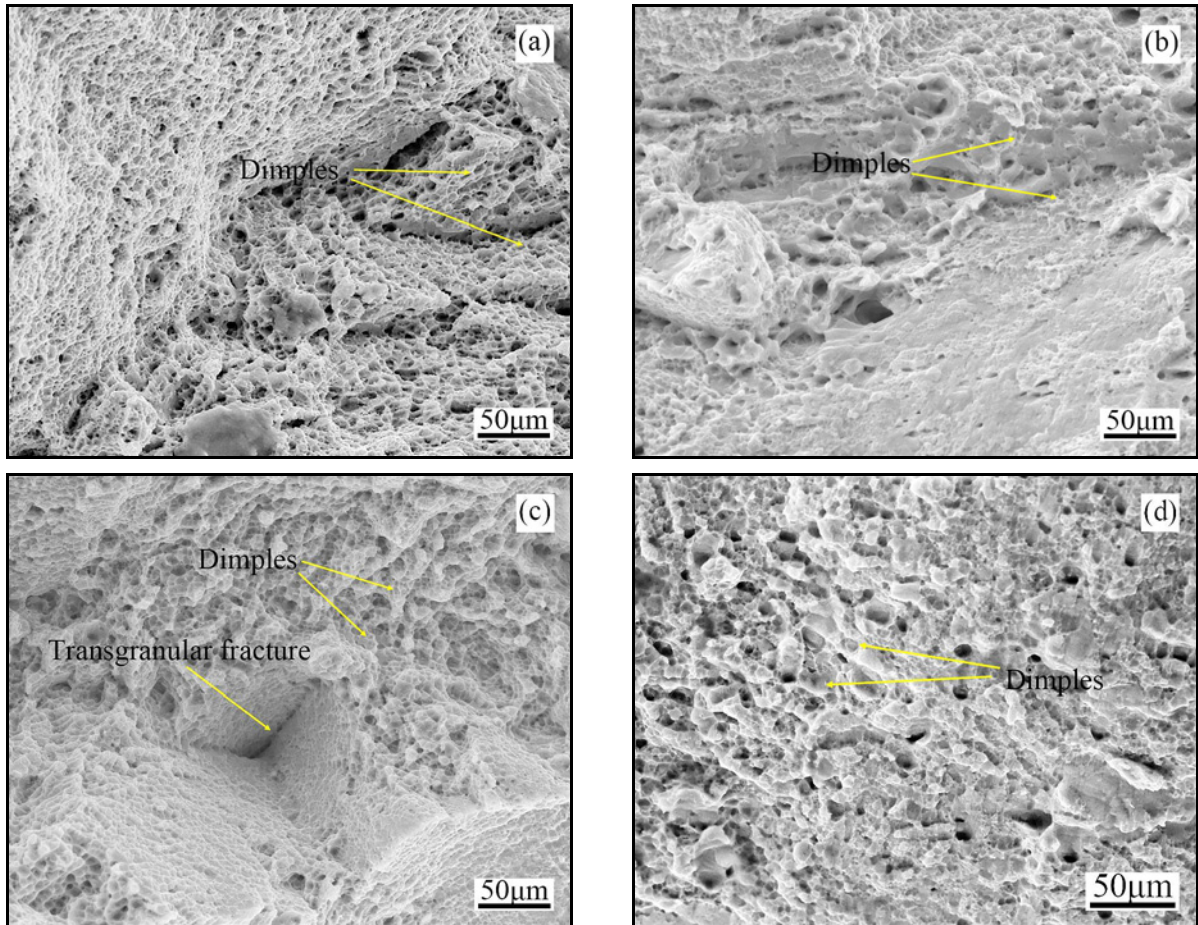


Fig. 10. Morphologies of tensile fracture surfaces at room temperature of (a) as-built, (b) AS-1, (c) DA-4, and (d) AS-4.

pin the grain boundaries [30, 31].

To further investigate the tensile properties of SLM-IN718, the morphology of the tensile fracture surfaces is shown in Fig. 10. Dimples can be seen in four specimens. In general, larger dimples indicate better plasticity. The DA-4 specimen with the smallest dimples shows a transgranular fracture structure

(Fig. 10c), which corresponds to poor plasticity but optimum strength. The  $\gamma''$  and  $\delta$  phases precipitated during the aging treatment play an important role in improving the strength. The AS-1 and AS-4 specimens have larger dimple structures and better ductility. Most precipitated phase is dissolved after 1000 °C solution treatment for 2 h. Almost only the matrix

phase is left in the alloy, so it has good plasticity. Parameters such as the type of load and temperature affect whether the material is brittle or ductile. However, metals with face-centered cubic structures are not affected by temperature because of their low yield strength and plentiful slip systems.

#### 4. Conclusions

Metallographic and XRD characterizations indicate that the precipitation of the  $\delta$  phase increases with aging time at 750°C. Meanwhile, the pre-precipitated  $\delta$  phase led to the fine grain morphology after 1000°C solution treatment. The specimen aged at 750°C for 48 h (DA-4) had the optimum hardness because of the precipitated  $\gamma''$  and  $\delta$  phase in the aging state. The specimens that experienced only solution treatment (AS-1) and aging at 750°C + solution treatment (AS-4) had the lowest hardness. AS-4 had better strength and plasticity than AS-1 because the  $\delta$  phase precipitated during the pre-aging treatment, causing the grains to get fine.

#### Acknowledgements

This work was financially supported by the Excellent Youth Exchange Program of the China Association for Science and Technology.

#### References

- [1] J. J. Shi, X. Li, Z. X. Zhang, G. H. Cao, A. M. Russell, Z. J. Zhou, C. P. Li, G. F. Chen, Study on the microstructure and creep behavior of Inconel 718 superalloy fabricated by selective laser melting, *Materials Science and Engineering A* 765 (2019) 138282. <https://doi.org/10.1016/j.msea.2019.138282>
- [2] Q. B. Jia, D. D. Gu, Selective laser melting additive manufacturing of Inconel 718 superalloy parts: Densification, microstructure and properties, *Journal of Alloys and Compounds* 585 (2014) 713–721. <https://doi.org/10.1016/j.jallcom.2013.09.171>
- [3] E. Hosseini, V. A. Popovich, A review of mechanical properties of additively manufactured Inconel 718, *Additive Manufacturing* 30 (2019) 100877. <https://doi.org/10.1016/j.addma.2019.100877>
- [4] P. Liu, J. Y. Hu, S. Y. Sun, K. Y. Feng, Y. B. Zhang, M. Q. Cao, Microstructural evolution and phase transformation of Inconel 718 alloys fabricated by selective laser melting under different heat treatment, *Journal of Manufacturing Processes* 39 (2019) 226–232. <https://doi.org/10.1016/j.jmapro.2019.02.029>
- [5] V. A. Popovich, E. V. Borisov, A. A. Popovich, V. Sh. Sufiarov, D. V. Masaylo, L. Alzina, Impact of heat treatment on mechanical behaviour of Inconel 718 processed with tailored microstructure by selective laser melting, *Materials & Design* 131 (2017) 12–22. <https://doi.org/10.1016/j.matdes.2017.05.065>
- [6] J. Li, Z. Y. Zhao, P. K. Bai, H. Q. Qu, B. Liu, L. Li, L. Y. Wu, R. G. Guan, H. Liu, Z. H. Guo, Microstructural evolution and mechanical properties of IN718 alloy fabricated by selective laser melting following different heat treatments, *Journal of Alloys and Compounds* 772 (2019) 861–870. <https://doi.org/10.1016/j.jallcom.2018.09.200>
- [7] J. J. Ruan, N. Ueshima, K. Oikawa, Phase transformations and grain growth behaviors in superalloy 718, *Journal of Alloys and Compounds* 737 (2018) 83–91. <https://doi.org/10.1016/j.jallcom.2017.11.327>
- [8] K. W. Chen, H. Li, C. H. Lim, N. Jia, W. L. Yan, Fine grains within narrow temperature range by tuning strain-induced boundary migration dominated recrystallization for selective laser melted Inconel 718, *Scripta Materialia* 219 (2022) 114882. <https://doi.org/10.1016/j.scriptamat.2022.114882>
- [9] G. Q. Wang, M. S. Chen, H. B. Li, Y. C. Lin, W. D. Zeng, Y. Y. Ma, Methods and mechanisms for uniformly refining deformed mixed and coarse grains inside a solution-treated Ni-based superalloy by two-stage heat treatment, *Journal of Materials Science & Technology* 77 (2021) 47–57. <https://doi.org/10.1016/j.jmst.2020.11.030>
- [10] X. Yang, B. X. Wang, W. Jiang, S. N. Chen, J. Wang, The superplasticity improvement of Inconel 718 through grain refinement by large reduction cold rolling and two-stage annealing, *Materials Science and Engineering A* 823 (2021) 141713. <https://doi.org/10.1016/j.msea.2021.141713>
- [11] C. Ruiz, A. Obabueki, K. Gillespie, Evaluation of the microstructure and mechanical properties of delta processed alloy 718, superalloys, TMS, Warrendale PA 1992, pp 33–42. ISSN 0142–1123
- [12] S. Azadian, L. Y. Wei, R. Warren, Delta phase precipitation in Inconel 718, *Materials Characterization* 53 (2004) 7–16. <https://doi.org/10.1016/j.matchar.2004.07.004>
- [13] J. J. Ruan, N. Ueshima, K. Oikawa, Growth behavior of the  $\delta$ -Ni<sub>3</sub>Nb phase in superalloy 718 and modified KJMA modeling for the transformation-time-temperature diagram, *Journal of Alloys and Compounds* 814 (2020) 152289. <https://doi.org/10.1016/j.jallcom.2019.152289>
- [14] M. Cheng, H. Y. Zhang, S. H. Zhang, Microstructure evolution of delta-processed IN718 during holding period after hot deformation, *Journal of Materials Science* 47 (2011) 251–256. <https://doi.org/10.1007/s10853-011-5792-1>
- [15] J. Y. Zhang, B. Xu, N. ul Haq Tariq, M. Y. Sun, D. Z. Li, Y. Y. Li, An innovative approach for grain refinement in Ni-based superalloys: Modification in the classical delta process through  $\gamma''$  pre-aging treatment, *Journal of Alloys and Compounds* 818 (2020) 152827. <https://doi.org/10.1016/j.jallcom.2019.152827>
- [16] Z. Wang, K. Guan, M. Gao, X. Li, X. Chen, X. Zeng, The microstructure and mechanical properties of deposited-IN718 by selective laser melting, *Journal of Alloys and Compounds* 513 (2012) 518–523. <https://doi.org/10.1016/j.jallcom.2011.10.107>
- [17] H.-Y. Wan, Z.-J. Zhou, C.-P. Li, G.-F. Chen, G.-P. Zhang, Enhancing fatigue strength of selective laser melting-fabricated Inconel 718 by tailoring heat treatment route, *Advanced Engineering Materials* 20

- (2018) 180307.  
<https://doi.org/10.1002/adem.201800307>
- [18] S. Sui, J. Chen, Z. Li, H. S. Li, X. Zhao, H. Tan, Investigation of dissolution behavior of Laves phase in Inconel 718 fabricated by laser directed energy deposition, *Additive Manufacturing* 32 (2020) 1010555. <https://doi.org/10.1016/j.addma.2020.101055>
- [19] Z. F. Song, S. Gao, Z. Q. Wang, L. Lan, J. S. Hou, B. He, Effects of non-equilibrium microstructures on microstructure evolution and mechanical properties of laser powder bed fusion IN625 Ni-based superalloy during long-term thermal exposure at 700°C and 750°C, *Materials Science and Engineering A* 856 (2022) 143883. <https://doi.org/10.1016/j.msea.2022.143883>
- [20] V. Beaubois, J. Huez, S. Coste, O. Brucelle, J. Lacaze, Short term precipitation kinetics of delta phase in strain free Inconel\* 718 alloy, *Materials Science and Technology* 20 (2013) 1019–1026. <https://doi.org/10.1179/026708304225019830>
- [21] D. Cai, W. Zhang, P. Nie, W. Liu, M. Yao, Dissolution kinetics of  $\delta$  phase and its influence on the notch sensitivity of Inconel 718, *Materials Characterization* 58 (2007) 220–225. <https://doi.org/10.1016/j.matchar.2006.04.020>
- [22] C. Zhang, L. Yu, H. Wang, Kinetic analysis for high-temperature coarsening of  $\gamma''$  phase in Ni-based superalloy GH4169, *Materials (Basel)* 12 (2019) 2096. <https://doi.org/10.3390/ma12132096>
- [23] J. Zhang, Q. L. Zhang, D. Li, W. H. Tong, J. H. Yao, Z. B. Leng, Effect of  $\delta$  aging treatment on microstructure and tensile properties of repaired Inconel 718 alloy using laser additive manufacturing, *Chinese Journal of Lasers* 47 (2020) 66–73. <https://doi.org/10.3788/cjl202047.0102001>
- [24] Y. Gao, D. Zhang, M. Cao, R. Chen, Z. Feng, R. Poprawe, J. Henrich Schleifenbaum, S. Ziegler, Effect of  $\delta$  phase on high temperature mechanical performances of Inconel 718 fabricated with SLM process, *Materials Science and Engineering A* 767 (2019) 138327. <https://doi.org/10.1016/j.msea.2019.138327>
- [25] J. R. Zhao, F. Y. Hung, T. S. Lui, Microstructure and tensile fracture behavior of three-stage heat treated Inconel 718 alloy produced via laser powder bed fusion process, *Journal of Materials Research and Technology* 9 (2020) 3357–3367. <https://doi.org/10.1016/j.jmrt.2020.01.030>
- [26] M. Sundararaman, P. Mukhopadhyay, S. Banerjee, Precipitation and room temperature deformation behavior of Inconel 718, *SUPERALLOYS*, (1994), pp. 419–440. ISSN 0142-1123.
- [27] Y. N. Zhao, K. Guan, Z. W. Yang, Z. P. Hu, Z. Qian, H. Wang, Z. Q. Ma, The effect of subsequent heat treatment on the evolution behavior of second phase particles and mechanical properties of the Inconel 718 superalloy manufactured by selective laser melting, *Materials Science and Engineering A* 794 (2020) 139931. <https://doi.org/10.1016/j.msea.2020.139931>
- [28] F. C. Liu, X. Lin, M. H. Song, W. W. Zhao, J. Chen, W. D. Huang, Effect of intermediate heat treatment temperature on microstructure and notch sensitivity of laser solid formed Inconel 718 superalloy, *Journal of Wuhan University of Technology-Mater. Sci. Ed.* 26 (2011) 908–913. <https://doi.org/10.1007/s11595-011-0335-9>
- [29] M. Ni, S. C. Liu, C. Chen, R. D. Li, X. Y. Zhang, K. C. Zhou, Effect of heat treatment on the microstructural evolution of a precipitation-hardened superalloy produced by selective laser melting, *Materials Science and Engineering A* 748 (2019) 275–285. <https://doi.org/10.1016/j.msea.2019.01.109>
- [30] F. X. Zhang, D. Liu, Y. H. Yang, C. X. Liu, J. G. Wang, Z. Zhang, H. P. Wang, Investigation on the influences of  $\delta$  phase on the dynamic recrystallization of Inconel 718 through a modified cellular automaton model, *Journal of Alloys and Compounds* 830 (2020) 154590. <https://doi.org/10.1016/j.jallcom.2020.154590>
- [31] Q. Zhu, L. Cheng, C. Wang, G. Chen, H. Qin, P. Zhang, Effect of  $\delta$  phase on size effect in microtensile deformation of a nickel-based superalloy, *Materials Science and Engineering A* 766 (2019) 138405. <https://doi.org/10.1016/j.msea.2019.138405>